Mesh Optimization for the One-Way Helmholtz Equation in an Inhomogeneous Medium

Mikhail S. Lytaev(✉)

St. Petersburg Federal Research Center of the Russian Academy of Sciences, 14-th Linia, V.I., No. 39, Saint Petersburg 199178, Russia
mikelytaev@gmail.com

Abstract. This paper presents an algorithm for the automated selection of optimal computational grid parameters in finite-difference Padé approximations of the two-dimensional one-way Helmholtz equation in an inhomogeneous medium. Unlike previous works, where the optimization was performed for a homogeneous medium or accounted only for the propagation angle, the proposed algorithm explicitly takes into account the range of the local wavenumber. The grid steps along the longitudinal and transverse coordinates are selected so as to minimize the computational cost while maintaining a prescribed dispersion error tolerance. A tabulation-based implementation enables real-time grid selection. The algorithm is analyzed on two fundamentally different classes of problems: tropospheric radio wave propagation, where the wavenumber is nearly constant, and underwater acoustics, where it varies significantly between the water column and the sediment. It is demonstrated that ignoring the wavenumber variation leads to grids that are 10–40 times too sparse for underwater acoustics problems, resulting in unacceptable modeling errors.

Keywords: wave propagation · parabolic equation · mesh optimization · Padé approximation · refractive index · underwater acoustics · radio wave propagation

1 Introduction

Computer simulation of wave field propagation in inhomogeneous media is a fundamental problem in mathematical physics, arising in radiophysics [11], computational underwater acoustics (UWA) [5,9], atmospheric acoustics [3], medical ultrasound [18], seismology [7], and optics [2]. One of the most effective and versatile numerical approaches is the parabolic equation (PE) method, originally proposed by Leontovich and Fock [10] for tropospheric radio wave propagation (RWP). The PE method and its wide-angle generalizations, the one-way Helmholtz equation method [8], have become indispensable tools in applied wave physics, owing to their deterministic nature and high computational efficiency.

© The Author(s), under exclusive license to Springer Nature Switzerland AG 2027
O. Gervasi et al. (Eds.): ICCSA 2026, LNCS 16767, pp. 144–160, 2027.
https://doi.org/10.1007/978-3-032-30491-9_10

Modern implementations rely on the rational Padé approximation of the pseudo-differential propagation operator [1,6]. The accuracy and efficiency of the resulting numerical scheme depend critically on several computational parameters: the longitudinal grid step Δx, the transverse grid step Δz, the reference propagation constant β, and the order of the Padé approximation. Choosing a grid that is too coarse leads to unacceptable dispersion errors, while an unnecessarily dense grid wastes computational resources. In practice, these parameters are often selected manually, which is error-prone and prevents the integration of wave propagation solvers into automated pipelines.

The problem of automated parameter selection has been addressed in a series of works. In [12], presented at ICCSA 2020, the dispersion analysis of the finite-difference Padé scheme was used to formulate an optimization problem for the two-dimensional homogeneous case. In [14], presented at ICCSA 2023, the approach was extended to the three-dimensional case, including the alternating-direction implicit (ADI) splitting, and a formula for the optimal reference propagation constant was derived. In [13], it was shown that rational interpolation on an interval allows the use of sparser grids than the local Padé approximation. In [15], the mesh optimization problem for underwater acoustics in an inhomogeneous medium was analyzed using a numerical search over the reference sound speed.

However, the algorithms in [12–14] assumed a homogeneous medium ($k = \text{const}$), and the numerical search in [15] did not provide an explicit closed-form procedure or jointly optimize Δx and Δz. The present work addresses these limitations. The main contributions are:

1. An explicit optimization algorithm for the two-dimensional one-way Helmholtz equation that jointly determines β, Δx, and Δz accounting for the full range of the local wavenumber $k(x, z) \in [k_{\min}, k_{\max}]$. The optimization is performed with respect to the reference propagation constant β rather than the reference sound speed.
2. A practical tabulation-based implementation enabling real-time grid selection.
3. A comparative analysis on tropospheric radio wave propagation (where $k_{\min} \approx k_{\max}$) and underwater acoustics (where they differ significantly), demonstrating that the wavenumber range is the dominant factor in the latter case.

2 Problem Statement

Consider the two-dimensional scalar Helmholtz equation

$$\frac{\partial^2 \psi}{\partial x^2} + \frac{\partial^2 \psi}{\partial z^2} + k^2(x, z)\, \psi = 0, \tag{1}$$

where $\psi(x, z)$ is the wave field, x is the longitudinal coordinate, z is the transverse coordinate, $k(x, z) = 2\pi f / c(x, z)$ is the local wavenumber, f is the frequency, $c(x, z)$ is the spatially varying wave speed, and $\lambda = c/f$ is the wavelength.

The wave field is generated by the initial condition $\psi(0, z) = \psi_0(z)$, where ψ_0 represents the radiation source. The function ψ is subject to boundary conditions on the lower boundary (e.g., impedance) and the upper boundary (e.g., transparent). The wave propagation occurs predominantly in the positive x-direction.

The range of $k(x, z)$ differs fundamentally between the two application domains of interest. In tropospheric radio wave propagation, the refractive index $n = c_0/c(x, z) \approx 1$ to high precision (the modified refractivity deviates from unity by $O(10^{-4})$), so $k_{\min} \approx k_{\max}$. In underwater acoustics, the sound speed varies from $c \approx 1500\,\mathrm{m/s}$ (water) to $c \approx 1700$–$2000\,\mathrm{m/s}$ (sediment), so $k_{\min}/k_{\max}$ can be as low as 0.75, a much larger relative variation.

3 One-Way Helmholtz Equation and Its Numerical Solution

3.1 Transverse Discretization

Rewrite (1) as

$$\frac{\partial^2 \psi}{\partial x^2} + H\psi = 0, \qquad H\psi = \frac{\partial^2 \psi}{\partial z^2} + k^2(x, z)\,\psi. \tag{2}$$

The transverse Laplacian $\partial^2/\partial z^2$ is discretized by the Numerov scheme [17]:

$$\frac{\partial^2 u}{\partial z^2} \approx D_{\Delta z}\, u = \frac{1}{\Delta z^2}\,\delta^2 \left(1 + \alpha\,\delta^2\right)^{-1} u,$$

where $\delta^2 u_j = u_{j-1} - 2u_j + u_{j+1}$ and $\alpha = 0$ for the 2nd order scheme, $\alpha = 1/12$ for the 4th order scheme. Figure 1 shows the transverse discretization error as a function of k_z for both schemes. The 4th order scheme improves accuracy by approximately two orders of magnitude at no additional computational cost.

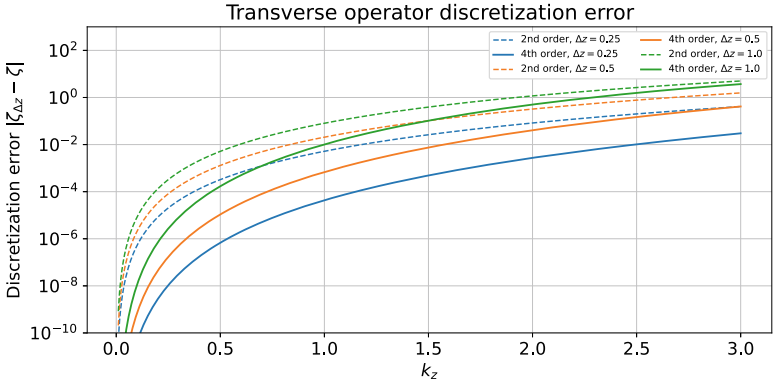

Fig. 1. Transverse operator discretization error for the 2nd and 4th order schemes at various Δz values.

3.2 Fourier Analysis and One-Way Factorization

Substituting the Fourier representation

$$\psi(x,z) = \frac{1}{\sqrt{2\pi}} \int_{-\infty}^{+\infty} \tilde{\psi}(x,k_z)\, e^{ik_z z}\, dk_z$$

into (2), the transverse operator acts on each Fourier component via its spectral symbol $\zeta(k_z)$:

$$e^{-ik_z z} \frac{\partial^2}{\partial z^2} e^{ik_z z} = -k_z^2,$$

$$e^{-ik_z z}\, D_{\Delta z}\, e^{ik_z z} = -\frac{1}{\Delta z^2}\left(4\sin^2\frac{k_z \Delta z}{2} + 16\alpha \sin^4\frac{k_z \Delta z}{2}\right). \tag{3}$$

Denoting the continuous symbol by $\zeta = -k_z^2$ and the discrete symbol by $\zeta_{\Delta z}$, the Helmholtz equation in the spectral domain reads

$$\frac{\partial^2 \tilde{\psi}}{\partial x^2} + \left(k^2(x,z) + \zeta\right)\tilde{\psi} = 0.$$

Factoring into forward- and backward-propagating components [5,8] and retaining the forward-propagating wave, we introduce the slowly varying envelope $u(x,z) = e^{-i\beta x}\psi(x,z)$. The step-by-step solution is

$$\tilde{u}(x + \Delta x, k_z) = P(\xi)\, \tilde{u}(x,k_z),$$

where

$$P(\xi) = \exp\left(i\tilde{\beta}\left(\sqrt{1+\xi} - 1\right)\right), \quad \tilde{\beta} = \beta \Delta x,$$

and

$$\xi = \frac{k^2(x,z) + \zeta}{\beta^2} - 1. \tag{4}$$

Here β is the reference propagation constant, a free parameter optimized by the algorithm (Sect. 4.3).

For the continuous operator, $\zeta = -k_z^2$ and $\xi = (k^2 - k_z^2)/\beta^2 - 1$, where $k_z = k\sin\theta$ for propagation angle θ. For the discrete operator, $\zeta = \zeta_{\Delta z}$ and

$$\xi_d = \frac{k^2(x,z) + \zeta_{\Delta z}}{\beta^2} - 1 = -\frac{4}{\beta^2 \Delta z^2}\left(\sin^2\frac{k_z \Delta z}{2} + 4\alpha \sin^4\frac{k_z \Delta z}{2}\right) + \frac{k^2(x,z)}{\beta^2} - 1. \tag{5}$$

The per-step error thus has two sources: (i) the *rational approximation error*, from approximating $P(\xi)$ (see below), and (ii) the *transverse discretization error*, from $\zeta \neq \zeta_{\Delta z}$, i.e., $\xi \neq \xi_d$.

3.3 Rational Padé Approximation

Following [6], we approximate the propagator by a rational function

$$P(\xi) \approx \tilde{P}(\xi) = \prod_{l=1}^{p} \frac{1 + a_l \xi}{1 + b_l \xi},$$

where a_l, b_l are the Padé coefficients of order $[m/n]$, $p = \max(m, n)$. Applying the inverse Fourier transform, the propagation step reduces to solving p tridiagonal systems:

$$\begin{cases} (1 + b_1 L)\, v_1 = (1 + a_1 L)\, u^{n-1}, \\ \quad \vdots \\ (1 + b_l L)\, v_l = (1 + a_l L)\, v_{l-1}, \qquad l = 2, \ldots, p-1, \\ \quad \vdots \\ (1 + b_p L)\, u^n = (1 + a_p L)\, v_{p-1}, \end{cases}$$

with transverse operator

$$Lu = \frac{1}{\beta^2} D_{\Delta z}\, u + \left(\frac{k^2(x,z)}{\beta^2} - 1 \right) u.$$

Throughout this paper, we use Padé approximations of order $[p-1, p]$, which are L-stable [4] and ensure attenuation of spurious high-frequency components.

4 Optimization Algorithm

4.1 Range of ξ in an Inhomogeneous Medium

From (4), the variable ξ ranges over

$$\xi \in \left[\frac{k_{\min}^2 - k_{z,\max}^2}{\beta^2} - 1,\ \frac{k_{\max}^2}{\beta^2} - 1 \right], \tag{6}$$

where $k_{\min} = \min_{x,z} k(x,z)$, $k_{\max} = \max_{x,z} k(x,z)$, and $k_{z,\max}$ is the maximum transverse wavenumber determined by the source. Note that the algorithm requires only these physical bounds; no artificial reference speed c_0 or reference wavenumber k_0 is needed.

This is the central observation of this paper: in an inhomogeneous medium, the ξ range depends not only on the maximum propagation angle $\theta_{\max}$ (through $k_{z,\max}$) but also on the ratio $k_{\min}/k_{\max}$. In tropospheric applications, $k_{\min} \approx k_{\max}$, so the range is essentially $[-\sin^2 \theta_{\max}, 0]$. In underwater acoustics, the term $k_{\min}^2/\beta^2 - 1$ can be much more negative (for $c_{\text{sed}} = 2000\,\text{m/s}$, $k_{\min}/k_{\max} \approx 0.75$), which dramatically widens the ξ interval. This is illustrated in Table 1.

Table 1. Range of ξ for various propagation angles and media. $\xi \in [\xi_{\min}, 0]$ where $\xi_{\min} = (k_{\min}/k_{\max})^2 - 1 - \sin^2\theta_{\max}$ (assuming $\beta = k_{\max}$).

$\theta_{\max}$	$\sin^2\theta_{\max}$	$\xi_{\min}$		
		RWP ($k_{\min} \approx k_{\max}$)	UWA ($c_{\text{sed}} = 1700$)	UWA ($c_{\text{sed}} = 2000$)
5°	0.008	−0.008	−0.229	−0.445
10°	0.030	−0.030	−0.252	−0.468
20°	0.117	−0.117	−0.338	−0.554
30°	0.250	−0.250	−0.471	−0.688
45°	0.500	−0.500	−0.721	−0.937

4.2 Error of the Rational Approximation

The absolute error of the rational approximation at each step is

$$R(\xi, \tilde{\beta}) = \left| P(\xi) - \prod_{l=1}^{p} \frac{1 + a_l \xi}{1 + b_l \xi} \right|.$$

Since the Padé approximation is centered at $\xi = 0$, the error increases monotonically with $|\xi|$ (Fig. 2). For each $\tilde{\beta}$ and threshold R_0, monotonicity guarantees the existence of bounds $\xi^- < 0 < \xi^+$ such that $R(\xi) \le R_0$ for all $\xi \in [\xi^-, \xi^+]$.

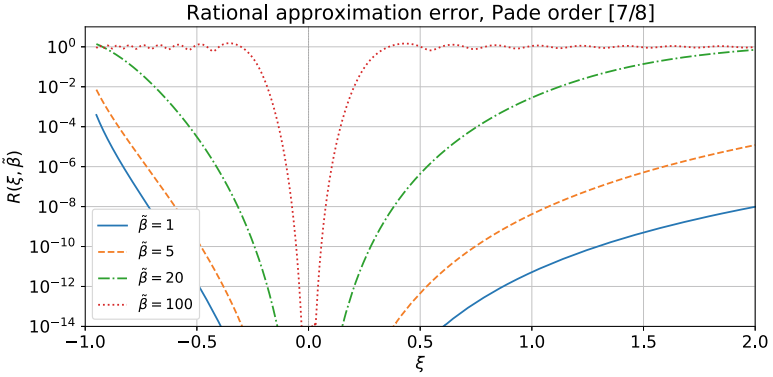

Fig. 2. Rational approximation error $R(\xi, \tilde{\beta})$ for Padé order [7/8]. The error is minimal near $\xi = 0$ and grows monotonically.

4.3 Constraints on β

For the rational approximation to be accurate over the full ξ range (6), we require $[\xi_{\min}, \xi_{\max}] \subseteq [\xi^-, \xi^+]$. This yields:

$$\beta \le \sqrt{\frac{k_{\min}^2 - k_{z,\max}^2}{\xi^- + 1}}, \qquad \beta \ge \sqrt{\frac{k_{\max}^2}{\xi^+ + 1}}. \tag{7}$$

A feasible β exists only when the lower bound does not exceed the upper bound. Among all feasible values, we select the smallest β, since the longitudinal step $\Delta x = \tilde{\beta}/\beta$ is maximized when β is minimized.

4.4 Transverse Discretization Error

From (4) and (5), the difference between the continuous and discrete ξ is

$$\Delta\xi = \xi - \xi_d = \frac{\zeta - \zeta_{\Delta z}}{\beta^2},$$

where ζ and $\zeta_{\Delta z}$ are the spectral symbols defined in (3). Explicitly,

$$|\Delta\xi| = \frac{1}{\beta^2}\left| k_z^2 - \frac{1}{\Delta z^2}\left(4\sin^2\frac{k_z\Delta z}{2} + 16\alpha\sin^4\frac{k_z\Delta z}{2}\right)\right|. \tag{8}$$

The impact of this discretization error on the propagator is estimated via

$$|P(\xi + \Delta\xi) - P(\xi)| \approx |P'(\xi)| \cdot |\Delta\xi|, \quad |P'(\xi)| = \frac{\tilde{\beta}}{2\sqrt{1+\xi}}.$$

The maximum of $|P'|$ on $[\xi^-, \xi^+]$ is at $\xi = \xi^-$. Requiring this error not to exceed R_0:

$$|\Delta\xi| \le \frac{2R_0\sqrt{1+\xi^-}}{\tilde{\beta}}. \tag{9}$$

Combining (8) and (9), the maximum allowable Δz is found by binary search.

4.5 Complete Procedure

The algorithm iterates over a precomputed table of candidate parameters $(\tilde{\beta}, R_0)$ and selects the combination maximizing $\Delta x \cdot \Delta z$ (minimizing computational cost) subject to the accumulated error constraint $\lceil x_{\max}/\Delta x \rceil \cdot R_0 < \varepsilon$.

The precomputed table uses grids $\mathcal{B} = \{0.01, 0.05, 0.1, \ldots, 50000\}$ (~ 50 values) and $\mathcal{R} = \{10^{-10}, \ldots, 10^{-5}\}$ (6 values), totaling $\sim$300 entries. The table depends only on the Padé order and can be reused across problems. The optimization loop performs only elementary arithmetic and at most one binary search per entry, completing in a fraction of a second. The proposed algorithm is implemented in the open-source Python library PyWaveProp [16].

5 Numerical Results

All results were obtained using PyWaveProp [16]. The 4th order Numerov scheme ($\alpha = 1/12$) is used throughout.

Algorithm 1. Grid optimization for the inhomogeneous PE.

Require: $k_{\min}$, $k_{\max}$, $k_{z,\max}$, ε, $x_{\max}$, Padé order $[m/n]$, transverse order α
Ensure: Optimal β, Δx, Δz

Precomputation (once per Padé order):
for all $\tilde{\beta} \in \mathcal{B}$, $R_0 \in \mathcal{R}$ **do**
  Compute $\xi^-(\tilde{\beta}, R_0)$ and $\xi^+(\tilde{\beta}, R_0)$ by binary search on $R(\xi, \tilde{\beta}) = R_0$
end for
Store table $\{(\tilde{\beta}, R_0) \mapsto (\xi^-, \xi^+)\}$

Optimization (for each problem instance):
$(\beta^*, \Delta x^*, \Delta z^*) \leftarrow (\mathrm{NaN}, 0, 0)$
for all $(\tilde{\beta}, R_0)$ in the table **do**
  Compute $\beta_{\max}$, $\beta_{\min}$ from (7)
  if $\beta_{\min} > \beta_{\max}$ **then**
    continue
  end if
  $\beta \leftarrow \beta_{\min}$, $\quad \Delta x \leftarrow \tilde{\beta}/\beta$
  if $\lceil x_{\max}/\Delta x \rceil \cdot R_0 > \varepsilon$ **then**
    continue
  end if
  Compute $\Delta\xi_{\max}$ from (9); find Δz by binary search on (8)
  if $\Delta x \cdot \Delta z > \Delta x^* \cdot \Delta z^*$ **then**
    $(\beta^*, \Delta x^*, \Delta z^*) \leftarrow (\beta, \Delta x, \Delta z)$
  end if
end for
return β^*, Δx^*, Δz^*

5.1 Tropospheric Radio Wave Propagation

Consider $f = 3$ GHz ($\lambda = 0.1\,\mathrm{m}$), $c \approx 3 \times 10^8\,\mathrm{m/s}$, $k_{\min} \approx k_{\max}$. Table 2 shows the optimal grid parameters computed by the algorithm for Padé order [7/8] and $\varepsilon = 10^{-3}$.

Table 2. Optimal grid for tropospheric propagation ($f = 3$ GHz, $n \approx 1$, Padé [7/8], $\varepsilon = 10^{-3}$).

$\theta_{\max}$	$x_{\max}$	Δx (m)	Δz (m)	$\Delta x/\lambda$	$\Delta z/\lambda$
3°	100 km	111.49	0.179	1114.9	1.79
5°	10 km	31.91	0.061	319.1	0.61
10°	10 km	8.03	0.009	80.3	0.09
20°	1 km	1.67	0.004	16.7	0.04
30°	1 km	1.19	0.002	11.9	0.02
45°	1 km	0.38	0.0004	3.8	0.004

For small propagation angles ($\theta_{\max} \leq 5°$), typical of long-range ducted propagation, the algorithm permits very large steps ($\Delta x \sim 300$–1100λ). The grid becomes rapidly denser with increasing angle. Since $k_{\min} \approx k_{\max}$, the wavenumber variation has no measurable effect on the optimization.

5.2 Underwater Acoustics: Full Algorithm vs. Homogeneous Assumption

Consider $f = 500\,\text{Hz}$ ($\lambda = 3\,\text{m}$), $c_{\text{water}} = 1500\,\text{m/s}$, $c_{\text{sed}} = 1700\,\text{m/s}$, $x_{\max} = 10\,\text{km}$, $\varepsilon = 10^{-3}$. Table 3 compares the *full algorithm* (which uses $k_{\min} \neq k_{\max}$) with the *homogeneous assumption* ($k_{\min} = k_{\max}$).

Table 3. Optimal grid for UWA ($f = 500\,\text{Hz}$, $c_{\text{sed}} = 1700\,\text{m/s}$, Padé [7/8], $\varepsilon = 10^{-3}$, $x_{\max} = 10\,\text{km}$). The homogeneous assumption overestimates Δx by a factor of 2–40.

$\theta_{\max}$	Full algorithm		Homogeneous assumption	
	$\Delta x/\lambda$	$\Delta z/\lambda$	$\Delta x/\lambda$	$\Delta z/\lambda$
5°	11.9	1.430	478.4	1.667
10°	10.4	0.485	112.4	1.667
20°	7.2	0.157	16.7	0.202
30°	5.6	0.081	11.9	0.103

The results reveal a dramatic difference. At $\theta_{\max} = 5°$, the homogeneous assumption suggests $\Delta x = 478.4\lambda$, while the full algorithm yields $\Delta x = 11.9\lambda$, a factor of **40**. At $\theta_{\max} = 10°$, the discrepancy is still more than tenfold. At larger angles, the angular contribution to the ξ range begins to dominate, and the discrepancy narrows to a factor of 2.

Using the homogeneous-assumption grid would result in dispersion errors far exceeding the prescribed tolerance, because the rational approximation is evaluated outside its region of accuracy. This error is systematic and cannot be compensated by reducing Δz alone.

Table 4. Same as Table 3, but for $f = 100\,\text{Hz}$ ($\lambda = 15\,\text{m}$).

$\theta_{\max}$	Full algorithm		Homogeneous assumption	
	$\Delta x/\lambda$	$\Delta z/\lambda$	$\Delta x/\lambda$	$\Delta z/\lambda$
5°	15.3	0.333	478.4	0.333
10°	13.7	0.333	112.4	0.333
20°	8.9	0.333	16.9	0.333
30°	5.6	0.182	13.7	0.333

For comparison, Table 4 shows results at $f = 100\,\mathrm{Hz}$ ($\lambda = 15\,\mathrm{m}$). The transverse discretization is less restrictive at this frequency, but the Δx discrepancy remains equally large.

5.3 Field Distribution: Correct vs Incorrect Grid

To demonstrate the practical consequences of ignoring the refractive index inhomogeneity, we compute the acoustic field in a layered shallow-water waveguide at $f = 1500\,\mathrm{Hz}$ ($\lambda = 1\,\mathrm{m}$). The water depth is 200 m with $c_{\mathrm{water}} = 1500\,\mathrm{m/s}$. Below the water column, a 100 m upper sediment layer ($c = 1700\,\mathrm{m/s}$) overlies a 50 m lower sediment layer ($c_{\mathrm{sed}} = 1800\,\mathrm{m/s}$); both sediment layers have $\rho = 1.5\ \mathrm{g/cm^3}$ and absorption $0.05\,\mathrm{dB}/\lambda$. A narrow Gaussian beam (1° width) is placed at 50 m depth with an elevation angle of −45° (steeply downward), giving $\theta_{\max} = 46°$. The propagation distance is $x_{\max} = 1\,\mathrm{km}$ and $\varepsilon = 0.1$.

Three computations are performed using the JAX-based solver [16] with Padé order [7/8]: (i) a reference solution on a fine grid ($\Delta x = 0.78\lambda$, $\Delta z = 0.011\lambda$; 426×10338 output points, downsampled 3× from the computational grid), (ii) the full optimization algorithm accounting for $k_{\min} \neq k_{\max}$ ($\Delta x = 2.4\lambda$, $\Delta z = 0.034\lambda$; 427×10338 points), and (iii) the homogeneous assumption with $k_{\min} = k_{\max}$ ($\Delta x = 5.7\lambda$, $\Delta z = 0.048\lambda$; 177×7309 points). The homogeneous grid is **2.4 times coarser** along the longitudinal coordinate than the correct grid, because the optimizer does not account for the wider ξ range caused by the sediment.

Figure 3 shows the two-dimensional field distribution for all three cases. The reference and the full-optimization solutions are visually indistinguishable, confirming that the optimized grid preserves the accuracy. The homogeneous-assumption solution, however, exhibits visible distortion of the beam pattern: the interference structure differs, and the field in the sediment layers is noticeably degraded.

Figure 4 compares the depth profiles of the field amplitude at three ranges: 250, 500, and 900 m. At 250 m, the three solutions are still close. By 500 m, the homogeneous-assumption curve begins to deviate. At 900 m, after the error has accumulated over many propagation steps, the deviation is pronounced: the interference pattern is shifted, and the amplitude deviates by up to several dB.

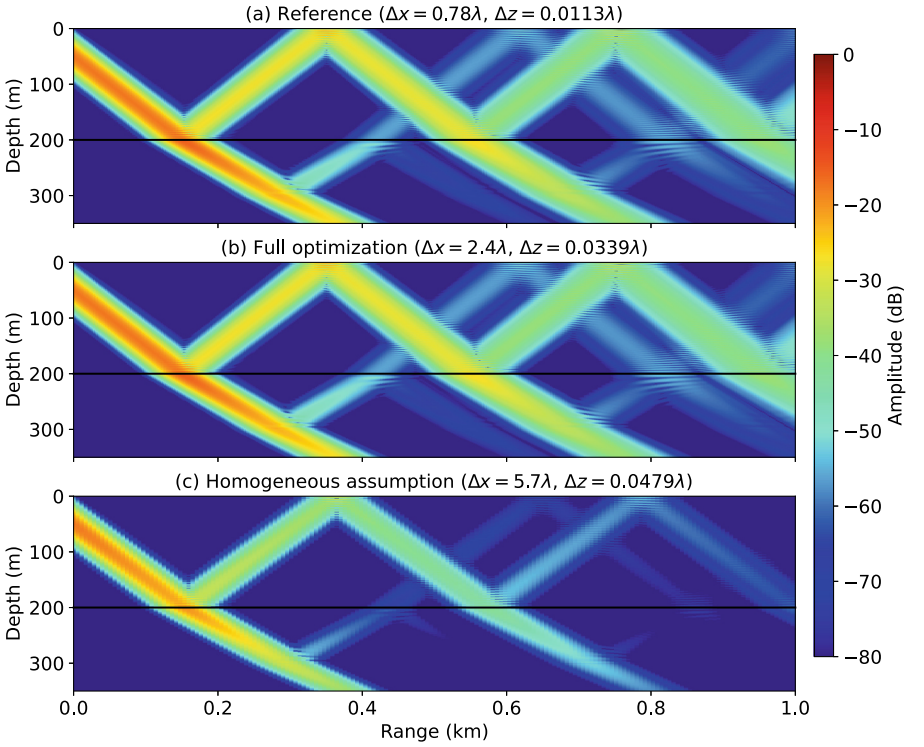

Fig. 3. Acoustic field amplitude (dB) in a layered waveguide ($f = 1500\,\text{Hz}$, c_{sed} up to 1800 m/s, range 1 km, $-45°$ beam). (a) Reference (fine grid). (b) Full optimization. (c) Homogeneous assumption (incorrect grid, 2.4× too sparse). The black line marks the sea bottom.

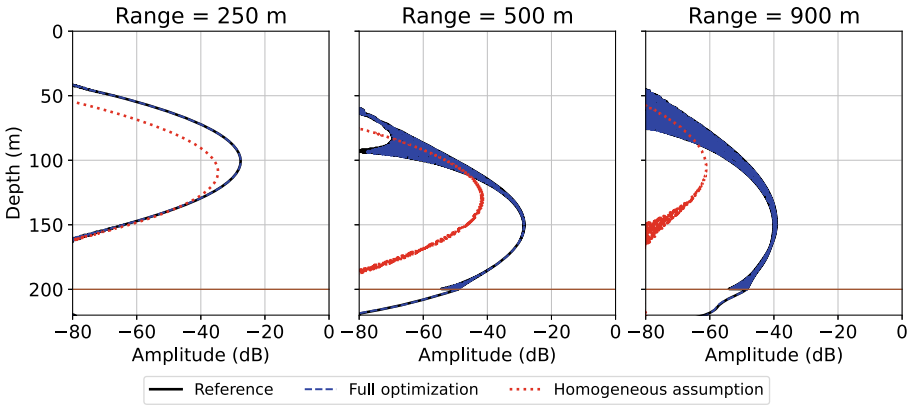

Fig. 4. Field amplitude vs. depth at ranges of 250, 500, and 900 m ($f = 1500\,\text{Hz}$, c_{sed} up to 1800 m/s, Padé [7/8], $-45°$ beam). The full-optimization curve (dashed blue) matches the reference (solid black); the homogeneous-assumption curve (dotted red) progressively diverges with increasing range. (Color figure online)

The range dependence of the error is shown in Fig. 5, which plots the transmission loss at 150 m depth as a function of range. The full-optimization curve tracks the reference over the entire 1 km range. The homogeneous-assumption curve diverges progressively, confirming that the dispersion error accumulates with each propagation step.

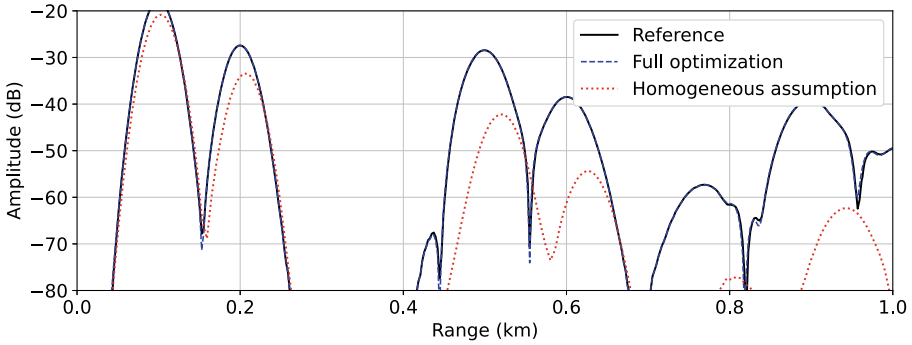

Fig. 5. Transmission loss at 150 m depth vs. range ($f = 1500$ Hz, c_{sed} up to 1800 m/s, Padé [7/8]). The homogeneous-assumption solution (dotted red) progressively diverges from the reference due to accumulated dispersion error. (Color figure online)

5.4 Effect of Sediment Sound Speed

Table 5 shows how the optimal grid depends on the sediment sound speed for $f = 500$ Hz, $\theta_{\max} = 10°$. As c_{sed} increases from 1500 m/s (homogeneous) to 2000 m/s, Δx decreases by a factor of 20. The sharpest drop occurs between 1500 and 1600 m/s, indicating that even a modest wavenumber contrast has a dramatic impact. This dependence is shown graphically in Fig. 6.

Table 5. Dependence of the optimal grid on c_{sed} ($f = 500$ Hz, $\theta_{\max} = 10°$, $x_{\max} = 10$ km).

c_{sed} (m/s)	$k_{\min}/k_{\max}$	$\Delta x/\lambda$	$\Delta z/\lambda$
1500 (homog.)	1.000	112.4	1.667
1600	0.938	16.7	0.557
1700	0.882	10.4	0.485
1800	0.833	7.2	0.435
1900	0.789	5.6	0.403
2000	0.750	5.6	0.397

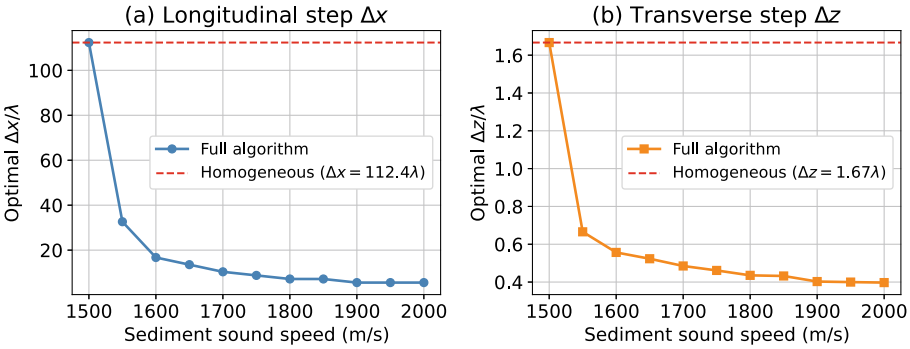

Fig. 6. Optimal grid steps vs. sediment sound speed ($f = 500\,\text{Hz}$, $\theta_{\max} = 10^\circ$, $x_{\max} = 10\,\text{km}$). The dashed line is the homogeneous assumption.

5.5 Optimal Δx as a Function of Propagation Angle

Figure 7 compares $\Delta x/\lambda$ as a function of $\theta_{\max}$ for the tropospheric and UWA cases. In both cases, Δx decreases with increasing angle, but the UWA curve lies significantly below the RWP curve due to the additional ξ-widening from the refractive index. The homogeneous assumption produces overly optimistic (too large) Δx values at all angles.

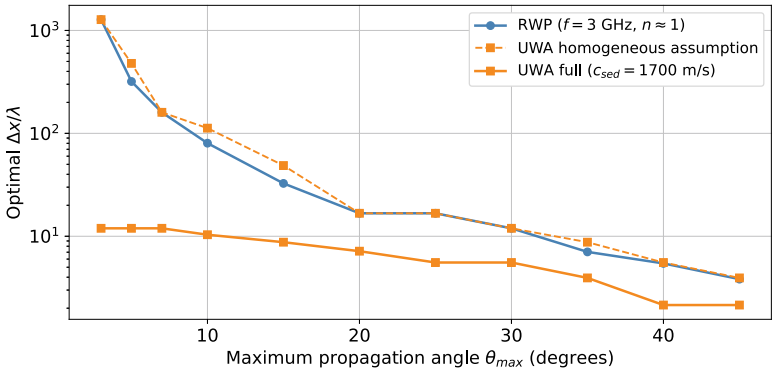

Fig. 7. Optimal $\Delta x/\lambda$ vs. $\theta_{\max}$ for RWP ($f = 3$ GHz) and UWA ($f = 500\,\text{Hz}$, $c_{\text{sed}} = 1700\,\text{m/s}$). Padé order [7/8], $\varepsilon = 10^{-3}$.

5.6 Comparison of Padé Orders

Table 6 shows the efficiency metric $V = p/(\Delta\,\mathrm{x} \cdot \Delta z)$ (lower is better, Δx and Δz in wavelengths) for the tropospheric case at various Padé orders and angles.

Table 6. Efficiency V for various Padé orders (tropospheric, $n \approx 1$, $\varepsilon = 10^{-3}$).

$\theta_{\max}$	$x_{\max}$	Order	$\Delta x/\lambda$	$\Delta z/\lambda$	V
3°	100 km	[1/2]	3.2	0.073	8.59
		[2/3]	31.9	0.231	4.08×10^{-1}
		[5/6]	477.8	0.810	1.55×10^{-2}
		[7/8]	1114.9	1.790	4.01×10^{-3}
10°	10 km	[2/3]	3.2	0.022	4.35×10^{1}
		[5/6]	48.1	0.075	1.66
		[6/7]	64.2	0.081	1.35
		[7/8]	80.3	0.085	1.17
20°	1 km	[2/3]	1.5	0.011	1.81×10^{2}
		[5/6]	14.8	0.036	1.14×10^{1}
		[7/8]	16.7	0.037	1.31×10^{1}

Table 7 presents the analogous comparison for UWA ($f = 500\,\mathrm{Hz}$, $c_{\mathrm{sed}} = 1700\,\mathrm{m/s}$, $\theta_{\max} = 10°$). Notably, orders [1/1] and [1/2] fail entirely in the UWA case, and the efficiency improves monotonically up to [7/8], suggesting that inhomogeneous environments benefit more from higher-order approximations. This is visualized in Fig. 8.

Table 7. Efficiency V for various Padé orders (UWA, $f = 500\,\mathrm{Hz}$, $c_{\mathrm{sed}} = 1700\,\mathrm{m/s}$, $\theta_{\max} = 10°$, $x_{\max} = 10\,\mathrm{km}$, $\varepsilon = 10^{-3}$).

Order	$\Delta x/\lambda$	$\Delta z/\lambda$	V
[2/3]	0.3	0.116	7.47×10^{1}
[3/4]	1.7	0.173	1.35×10^{1}
[4/5]	3.5	0.368	3.91
[5/6]	5.2	0.408	2.82
[6/7]	8.6	0.463	1.76
[7/8]	10.4	0.485	1.59

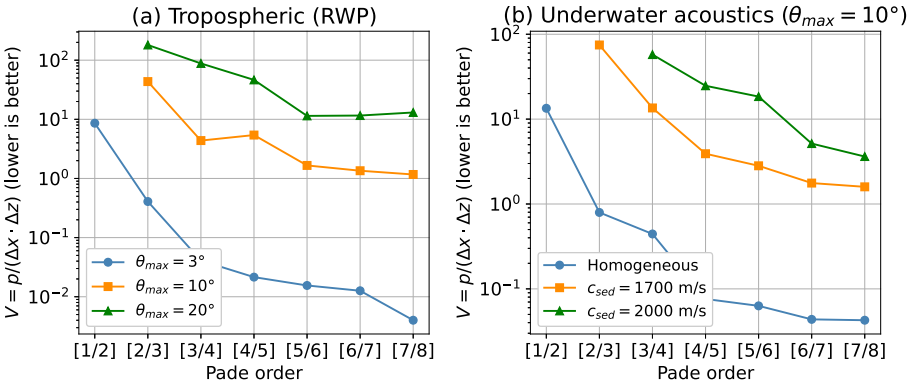

Fig. 8. Efficiency V vs. Padé order. (a) Tropospheric case at various angles. (b) UWA at $\theta_{\max} = 10°$ for different sediment speeds.

6 Conclusion

An algorithm for automated selection of optimal computational grid parameters for the two-dimensional parabolic equation in an inhomogeneous medium has been presented. The key results are as follows.

1. The range of the local wavenumber has been explicitly incorporated into the grid optimization procedure through the analysis of the variable ξ and its dependence on $k_{\min}$ and $k_{\max}$. The algorithm requires only these physical bounds; no artificial reference speed c_0 is needed. This extends the homogeneous-medium approach developed in [12,14].
2. For tropospheric radio wave propagation, where $k_{\min} \approx k_{\max}$, the wavenumber variation has negligible effect, and the optimization is governed by the propagation angle. The results are consistent with those obtained in [12,14].
3. For underwater acoustics, the wavenumber variation between water and sediment is the dominant factor. The homogeneous assumption leads to grids that are 10–40 times too sparse at small propagation angles, resulting in modeling errors far exceeding the prescribed tolerance.
4. A tabulation strategy enables real-time grid selection. The precomputed table depends only on the Padé order and can be reused across different problem instances.
5. Higher Padé orders are more beneficial in inhomogeneous environments: in the UWA case, the efficiency improves monotonically up to order [7/8], whereas in the tropospheric case, the optimal order is problem-dependent and may saturate at [5/6].

Future work includes the extension to three-dimensional inhomogeneous problems, range-dependent grid adaptation, and integration with inverse problem solvers where the wavenumber bounds are specified as an uncertainty interval.

Acknowledgments. This study was supported by the Russian Science Foundation grant No. 25-71-00028.

References

1. Baker, G.A., Graves-Morris, P.: Padé Approximants, 2nd edn. Cambridge University Press (1996)
2. Bekker, E.V., Sewell, P., Benson, T.M., Vukovic, A.: Wide-angle alternating-direction implicit finite-difference beam propagation method. J. Lightwave Technol. **27**(14), 2595–2604 (2009)
3. Bommidala, H., Colas, J., Emmanuelli, A., Dragna, D., Khodr, C., Cotté, B., Stevens, R.J.: Three-dimensional effects of the wake on wind turbine sound propagation using parabolic equation. J. Sound Vib. **608**, 119036 (2025)
4. Butcher, J.C.: Numerical Methods for Ordinary Differential Equations, 3rd edn. Wiley (2016)
5. Collins, M.D., Siegmann, W.L.: Parabolic Wave Equations with Applications. Springer, New York (2019). https://doi.org/10.1007/978-1-4939-9934-7
6. Collins, M.D.: A split-step padé solution for the parabolic equation method. J. Acoust. Soc. America **93**(4), 1736–1742 (1993)
7. Collins, M.D., Siegmann, W.L.: Parabolic equation techniques for seismology, seismo-acoustics, and arctic acoustics. J. Theoret. Comput. Acoust. **29**(02), 2130003 (2021)
8. Fishman, L., McCoy, J.J.: Derivation and application of extended parabolic wave theories. I. The factorized Helmholtz equation. J. Math. Phys. **25**(2), 285–296 (1984)
9. Jensen, F.B., Kuperman, W.A., Porter, M.B., Schmidt, H., Tolstoy, A.: Computational Ocean Acoustics, vol. 2011. Springer, New York (2011). https://doi.org/10.1007/978-1-4419-8678-8
10. Leontovich, M.A., Fock, V.A.: Solution of the problem of propagation of electromagnetic waves along the earth's surface by the method of parabolic equation. J. Phys. USSR **10**, 13–24 (1946)
11. Levy, M.F.: Parabolic Equation Methods for Electromagnetic Wave Propagation. IET (2000)
12. Lytaev, M.S.: Automated selection of the computational parameters for the higher-order parabolic equation numerical methods. In: Gervasi, O., et al. (eds.) ICCSA 2020. LNCS, vol. 12249, pp. 296–311. Springer, Cham (2020). https://doi.org/10.1007/978-3-030-58799-4_22
13. Lytaev, M.S.: Rational interpolation of the one-way Helmholtz propagator. J. Comput. Sci. **58**, 101536 (2022)
14. Lytaev, M.S.: Computational grid optimization for the 3D higher-order parabolic equation. In: Gervasi, O., et al. (eds.) Computational Science and Its Applications, ICCSA 2023. LNCS, pp. 170–185, vol. 13956. Springer, Cham (2023). https://doi.org/10.1007/978-3-031-36805-9_12
15. Lytaev, M.S.: Mesh optimization for the acoustic parabolic equation. J. Mar. Sci. Eng. **11**(3), 496 (2023)
16. Lytaev, M.S.: PyWaveProp: Python library for wave propagation modeling (2026). https://github.com/mikelytaev/wave-propagation

17. Lytaev, M.S.: Numerov-Padé scheme for the one-way Helmholtz equation in tropospheric radio-wave propagation. IEEE Antennas Wirel. Propag. Lett. **19**(12), 2167–2171 (2020)
18. Yuldashev, P., et al.: Numerical models of nonlinear acoustic wave propagation in medical ultrasound problems and certain applications of aeroacoustics and underwater acoustics. Mosc. Univ. Phys. Bull. **80**(2), 195–225 (2025)